CHEMISTRY OF MATERIALS

ARTICLE

pubs.acs.org/cm

Air Stable, Efficient Hybrid Photovoltaic Devices Based on Poly(3-hexylthiophene) and Silicon Nanostructures

Fute Zhang,[†] Baoquan Sun,[*,†] Tao Song,[†] Xiulin Zhu,[‡] and Shuittong Lee[§]

[†]Jiangsu Key Laboratory for Carbon-Based Functional Materials & Devices, Institute of Functional Nano & Soft Materials (FUNSOM), and [‡]Key Laboratory of Organic Synthesis of Jiangsu Province, School of Chemistry, Chemical Engineering and Materials Science, Soochow University, 199 Ren'ai Road, Suzhou, 215123, China

[§]Center of Super-Diamond and Advanced Films (COSDAF) and Department of Physics and Materials Science, City University of Hong Kong, Hong Kong SAR

Supporting Information

ABSTRACT: Efficient, stable hybrid photovoltaic (PV) devices based on poly(3-hexylthiophene) (P3HT) and silicon nanowire arrays (SiNWs) are reported. A two-step, chlorination/methylation procedure is used to convert Si−H bonds into Si−C ones to reduce the velocity of charge recombination at the silicon surface as well as achieve a favorable alignment of band-edge energies. In addition, Pt nanodots (PtNDs) are deposited onto the surface of the SiNWs to further tune the band-edge alignment and passivate nonmethylated silicon sites. Methylated silicon surfaces modified with PtNDs possess a favorable internal electric field in accord with expectations based on the electron affinity (~3.7 eV) and net positive surface dipole measured on such surfaces by ultraviolet photoemission spectroscopy. This attests to the degree of chemical control that can be exerted over the internal electric field in such systems by surface functionalization. In concert with methyl termination and decoration with PtNDs, hybrid PV devices based on composites of SiNWs and P3HT achieve an external quantum efficiency (EQE) of 76% at 800 nm and a power conversion efficiency (PCE) of 5.9% under simulated air mass 1.5 solar irradiation at 100 mW cm^{-2}. Moreover, these devices exhibit stable performance for more than 1200 h. In contrast, devices based on composites of hydrogen-terminated planar silicon and P3HT display an EQE of 0.19% at 560 nm and PCE of 0.006%. The ~800 times enhancement in device performance and improvement in stability are assigned to the facile derivatization of the surface of silicon nanostructures.

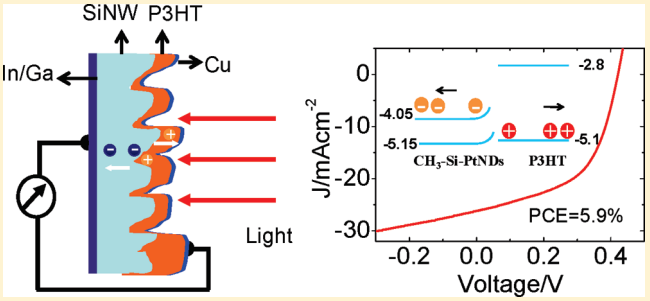

KEYWORDS: silicon nanowire arrays, poly(3-hexylthiophene), photovoltaic device, surface modification, charge recombination

INTRODUCTION

Composites of conjugated polymers and inorganic nanostructures have attracted wide interest because they can combine the desirable properties of both materials to produce efficient hybrid photovoltaic (PV) devices.[1−4] Conjugated polymers are readily processed to form films of large area, and their absorption coefficients are large so that only thin films are required for light harvesting in PV devices. The electronic and optical properties of inorganic nanostructures can be tuned simply by changing their dimensional shape and size, leading to efficient light harvesting and charge transport. The bandgap and offset of conjugated polymers and inorganic nanostructures are such that charges are separated across the organic/inorganic interface. The effects of the shape of the inorganic semiconductor nanocrystals, choice of conjugated polymer, and fabrication process on device performance have been investigated in detail, leading to a current state-of-the-art power conversion efficiency (PCE) of 3.1%.[5] A multitude of PV structures have been developed by combining conjugated polymers with various inorganic nanostructures such as CdSe,[5,6] TiO_2,[7,8] ZnO,[9] PbS,[10] PbSe,[11] Ge[12] and Si[13−17] to achieve highly efficient charge separation/transport.

Si nanowire arrays (SiNWs) showing highly ordered orientation are interesting one-dimensional nanostructures with specific optical and electrical properties.[18−30] The unique structure of SiNWs with a large surface area to volume ratio produces efficient light harvesting and charge separation/transport properties, which have been used in PV devices.[17−25,31] SiNWs offer an optimum optical path for efficient light harvesting along the long axial direction, while generated carriers are transported in the short radial direction (ca. micrometers), which decreases the velocity of charge recombination.[32] In addition, SiNWs display extended near-infrared absorption and enhanced light trapping capabilities over a wide range of incident angles compared with bulk materials.[19] SiNWs may allow high performance PV devices to be realized using low-purity Si with the short minority carrier diffusion length that is associated with thin sheet absorbers.[33] They also provide new opportunities to improve the PCE and to reduce the cost of PV devices. Indeed, a theoretical model has shown that, in

Received: November 9, 2010
Revised: March 6, 2011
Published: March 18, 2011

principle, devices with a radial junction geometry can yield PCE of greater than 15% even using silicon with a minority carrier length of less than 10 μm.[34] However, rapid carrier recombination at the surface/interface of SiNWs, because of their large surface-to-volume ratio, is a major problem.[21,35] Hybrid devices containing hydrogen-terminated silicon (H−Si) surfaces were unstable and oxidized gradually upon exposure to ambient conditions, which resulted in the loss of surface passivation.

In traditional PVs containing bulk materials, a thin native oxide SiO_x layer was introduced to suppress the velocity of recombination and has been documented that this velocity can be decreased to as low as 3 cm s^{-1}.[36,37] However, the thickness of the SiO_x layer, which formed instantaneously on SiNWs surfaces upon exposure to air, gradually increased over time and became a charge injection/transport barrier in these hybrid devices. To date, a cell based on a silicon film combined with the conjugated polymer poly(3-hexylthiophene) (P3HT) has yielded the highest PCE for this type of device of 1.16%.[15,38]

In this work, the silicon surface was modified to enhance the performance of hybrid heterojunction PV devices, where P3HT acts as donor. The methyl groups were used to passivate the dangling bonds on the silicon surface as well as tune the band-edge alignment of the surface. Charge recombination at the Si/P3HT interface was suppressed by converting Si−H bonds to Si−C ones. Furthermore, the optimum energy offset enhances charge transfer at the methylated silicon surface. Meanwhile, adjacent nonalkylated silicon sites were decorated with platinum nanodots (PtNDs) via electrochemical deposition. Methylated silicon (CH_3−Si) surfaces modified with PtNDs possessed a favorable internal electric field because of their electron affinity (3.7 eV) and net positive surface dipole. Hybrid organic PV devices based on CH_3−SiNWs and containing PtNDs achieved a PCE of 5.9% under irradiation with a simulated air mass (AM) 1.5 solar spectrum at 100 mW cm^{-2}, compared with a PCE of 0.006% from a device based on planar H−Si lacking PtNDs. Furthermore, the CH_3−SiNWs/PtNDs device showed negligible decay in PCE after operation for 1200 h. The high PCE and good stability of these devices are ascribed to the functionalization of the silicon surface.

EXPERIMENTAL SECTION

Materials. Hydrofluoric acid (HF), tetrahydrofuran (THF), chlorobenzene (CB), and phosphorus pentachloride (PCl_5) were purchased from Sinopharm Chemical Reagent Co., Ltd., China. Methyl magnesium chloride (CH_3MgCl) in THF was purchased from Alfa Aesar and used as received. Hexachloroplatinic (IV) acid (H_2PtCl_6) and lithium perchlorate ($LiClO_4$) were purchased from Aldrich. Deionized water (DI) with a resistivity of 18 MΩ·cm was purified using a Nanopure Diamond system.

Preparation of SiNWs. SiNWs were prepared using a previously reported method by metal ion-assisted electroless etching.[39] Clean n-type Si (100) substrates (resistivity of ~5 Ω·cm) were immersed in aqueous solution of HF (4.8 M) and $AgNO_3$ (0.02 M) for 30 min at 50 °C. The substrates were dipped in aqueous solution of HNO_3 (30% w/w) and then rinsed with DI water to remove any residual silver. To shorten the length of the SiNWs, the substrates were treated ultrasonically in DI water for 10 min and then rinsed with DI water. These steps were repeated five times to obtain short SiNWs.

Surface Modification. H−Si substrates were prepared by wet chemical etching in aqueous HF (5 M) with gentle shaking for 15 min. Then they were immersed in DI water for 1 min and dried under a stream of N_2 gas. The H−Si substrates were immediately transferred into glovebox. CH_3−Si substrates were fabricated following a two-step chlorination/alkylation method.[40] First, freshly prepared H−Si substrates were immersed in a saturated solution of PCl_5 in CB for 50 min at 90 ± 10 °C under N_2 to convert the Si−H bonds into Si−Cl ones. The Si−Cl samples were then rinsed sequentially with CB and THF three times. In the second step, the Si−Cl substrates were subsequently immersed in a solution of CH_3MgCl (1 M) in THF for at least 8 h at 70 ± 10 °C and then rinsed with THF. The samples were removed from the glovebox, dipped in DI water for 10 min, and then rinsed sequentially with acetone and ethanol.

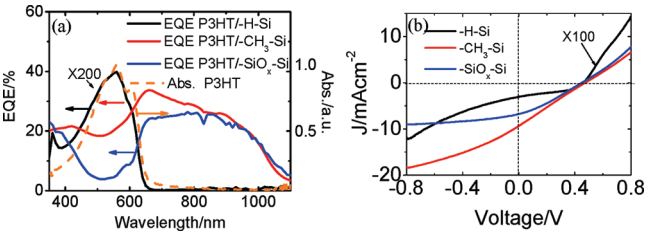

Figure 1. (a) Optical absorption spectra of P3HT films and EQE of hybrid devices containing planar silicon with various surface modifications. For comparison, EQE values of the P3HT/−H−Si device are magnified 200 times. (b) $I-V$ curves of hybrid devices containing planar silicon with various surface modifications. The current density of the P3HT/−H−Si device is magnified 100 times.

To deposit PtNDs onto the silicon substrates, the substrates were bonded with copper wire and submerged in an electrolyte consisting of H_2PtCl_6 (5 mM) and $LiClO_4$ (100 mM) in ethanol. A Pt plate acted as a counter electrode. A bias voltage of 0.8 V was applied between the two electrodes for 3 min.

Characterization of SiNWs. The light reflection ratio of the substrates was measured using a spectrometer (Perkin-Elmer Lambda 700) fitted with an integrating sphere. The morphology of the SiNWs was investigated using a high resolution scanning electron microscope (SEM, FEI Quanta 200 FEG). X-ray photoelectron spectroscopy (XPS) and ultraviolet photoelectron spectroscopy (UPS) were performed with a Shimadzu ESCA-1000 spectrometer and a KRATOS-AXIS-165 spectrometer using a Mg Kα line, respectively.

Fabrication and Characterization of PV Devices. P3HT films were deposited onto Si substrates by spin-coating a solution of P3HT (15 mg/mL) in CB. The substrates were annealed in glovebox at 150 °C for 30 min. Semitransparent Cu electrodes patterned using a shadow mask were thermally evaporated onto the P3HT films. Indium−gallium alloy (In/Ga) was attached onto the rear side of the substrates to obtain an Ohmic contact. External quantum efficiency (EQE) measurements were obtained by dispersing the emission from a xenon lamp through a Newport monochromator and focusing it on a device pixel with an area of 4 mm^2. A Newport 91160 solar simulator equipped with a 300 W xenon lamp and an AM 1.5 filter was used as an irradiation source to generate a simulated solar spectrum. The irradiation intensity was 100 mW cm^{-2}, which was calibrated by a standard silicon PV device (91150, Newport).

RESULTS AND DISCUSSION

Hydrogen-Terminated (−H) Planar Silicon Electrodes. A hybrid PV device based on a composite of P3HT and silicon nanospheres (1−10 nm in size) demonstrated a PCE of 1.16%,[15,35,38] indicating that there was strong intercoupling between silicon and P3HT. In this device,[15] excitons generated electrons and holes via charge separation at the Si/P3HT interface. Meanwhile, the individual continuous networks of both the

Scheme 1. Electron Energy Levels and Energy-Band Diagrams (numbers are in eV) from the Semiconductor Outwards into the Molecular or Silicon Oxide Layer[a]

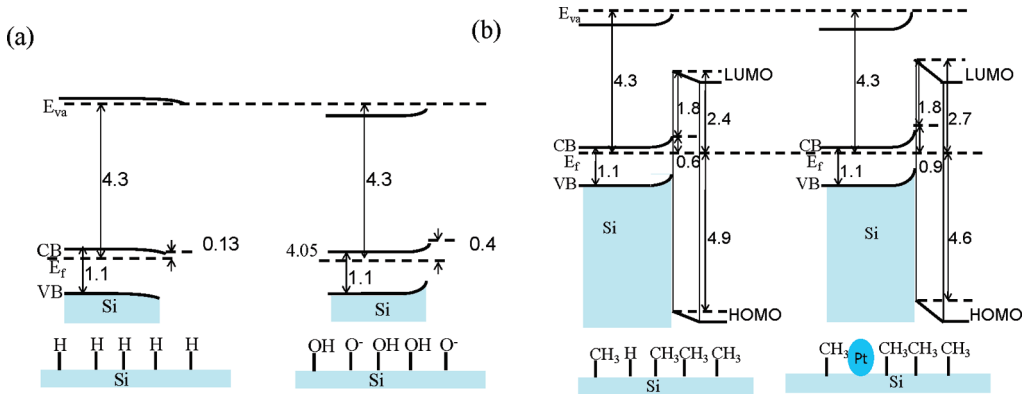

[a] Numbers were obtained from UPS measurements and related references. (a) Left: −H−Si molecular junction; right: $-SiO_x-Si$ junction. (b) Left: $-CH_3-Si$ molecular junction; right: $-CH_3-Si$(Pt) molecular junction. In (b), a HOMO−LUMO gap for the Si/methyl group system formed from interactions between the frontier orbitals of the methyl groups and the surface state levels of Si (see text for explanation). CB: conducting band; VB: valence band; E_f: Fermi energy; E_{va}: vacuum energy; E_f of silicon was calculated based on a silicon doping concentration of 10^{15} cm^{-3} (~5 Ω·cm resistivity).

silicon nanospheres and P3HT allowed photogenerated carriers to be collected by their corresponding electrodes. The same charge transfer process could also occur at a bulk Si/P3HT interface. However, unfortunately the freshly prepared hydrogen-terminated silicon (−H−Si)/P3HT hybrid device displayed very poor PV performance, as shown in Figure 1. The EQE was only 0.19% at the maximum absorption of the P3HT film (560 nm). Meanwhile, the short circuit current density (J_{sc}) of 0.03 mA cm^{-2}, open circuit voltage (V_{oc}) of 0.458 V, and fill factor (FF) of 0.39 yielded a PCE of just 0.006%, which was extremely low. A plot of EQE vs wavelength mimicked the profile of the absorption spectrum of P3HT, which indicated that only light harvested by P3HT generated photocurrent.

The poor performance of the −H−Si/P3HT device was attributed to charge recombination at the organic−inorganic interface as well as an unfavorable internal electric field, as shown in Scheme 1a. It has been reported that −H−Si surfaces display a high velocity of surface recombination (up to 500 cm/s).[38] In addition, the negative polarity of the −H−Si surface leads the reverse internal electric field for promoting electron movement toward the cathode, as shown in Scheme 1a. In principle, a covalently bonded passivation layer on silicon can either raise or lower the effective electron affinity at the surface, depending on the sign of the associated dipole. The magnitude of the electron affinity at the surface shifts relative to that in the bulk by an amount equal to ΔE_{dipole}.[41] The electron affinity of bulk Si is 4.05 eV,[42] and synchrotron photoemission studies have indicated that a −H−Si surface possesses a net negative surface dipole of 0.12 eV that arises from the formation of Si−H bonds,[42] as illustrated in Scheme 1a. Hence, the −H−Si surface possesses an electron affinity of 4.17 eV. Although the silicon film absorbed light, the electrons and holes produced recombined immediately because of the reverse internal electric field, without forming a photocurrent. This phenomenon was not observed in a previously reported device based on Si/P3HT composites.[14−16] We believe that this difference was caused by the use of a fresh H−Si surface, which was free of SiO_x. To avoid any generation of SiO_x, all experiments were performed in a glovebox (H_2O < 1 ppm, O_2 < 1 ppm), except for the silicon surface etching and hydrogen termination steps. A higher PV performance was obtained once the −H−Si surface was exposed to air for less than 30 min.

Silicon Oxide-Terminated ($-SiO_x$) Planar Silicon Electrodes. It is well-known that a thin layer of SiO_x can behave as an efficient passivation layer for silicon because of the low velocity of recombination at its surface. As shown in Figure 1, the performance of the hybrid device $-SiO_x-Si$/P3HT was dramatically improved compared with the −H−Si/P3HT device, consistent with previous reports.[14−16] Furthermore, the formation of SiO_x reversed the direction of the internal electric field, which promoted the movement of electrons toward the cathode. As shown in Scheme 1a, the offset of the surface band bending of $-SiO_x-Si$ became positive by ca. 0.15 eV compared with the negative value for −H−Si (−0.12 eV),[41] because of the negative dipole of silicon oxide.

An EQE spectrum of the $-SiO_x-Si$/P3HT device showed that a photocurrent was generated by silicon because the device displayed a photocurrent over the whole spectrum (350−1100 nm). Between 400 and 650 nm where the P3HT film absorbed, the EQE decreased because of an optical effect of P3HT. In organic/inorganic hybrid systems, excitons generated in the organic composite need to diffuse to the interface, where charge separation takes place. However, because the exciton diffusion length in P3HT is only ~10 nm,[2,43−46] only excitons generated in P3HT within ~10 nm of the P3HT/silicon interface could reach the interface. In these devices, the P3HT layer was ~50 nm thick to form a continuous film. Between 500 and 650 nm, a large proportion of the light was harvested by P3HT instead of Si. However, only part of this absorbed light can generate a photocurrent because of the limited exciton diffusion length of P3HT. For light absorbed by silicon, the generated electrons reach the cathode while holes are injected into the P3HT under the driving force of the internal electric field. The current−voltage ($I-V$) curve of the $-SiO_x-Si$/P3HT device revealed a J_{sc} of 6.8 mA cm^{-2}, V_{oc} of 0.458 V and FF of 0.39, giving a PCE of 0.9%. J_{sc} improved by ~200 times upon the formation of SiO_x at the interface because of the generation of a favorable internal electric field.

The critical role of the passivation layer was verified by investigating the dependence of J_{sc} on the in situ formation of

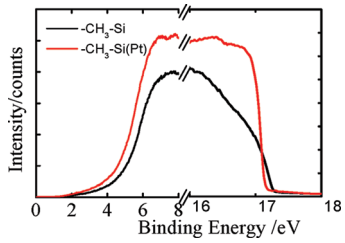

Figure 2. UPS analysis of methylated silicon with and without electrochemically deposited PtNDs.

SiO_x, as shown in Figure S1 in the Supporting Information. The uncapsulated −H−Si/P3HT device and a fresh −H−Si substrate were irradiated under light with an intensity of 100 mW cm^{-2}. A source meter was used to measure J_{sc} over time. Meanwhile, an ellipsometer was used to measure the thickness of SiO_x on the fresh −H−Si surface. A very small J_{sc} was detected when the −H−Si/P3HT device was first removed from the glovebox. However, after just 10 s of irradiation, J_{sc} increased by 100 times because a SiO_x layer with a thickness of 1.8 Å had formed. As time elapsed, the current reached saturation. A monolayer of SiO_x forms on a H−Si surface after exposure to air for 1 h and can last for several weeks in the dark. Here, the exposure to intense light accelerated the formation of the SiO_x layer.

Although it was convenient to form a SiO_x layer to enhance performance of the hybrid Si/P3HT device, some disadvantages limited the use of this tactic. The formation of SiO_x via light illumination was dependent on the crystal orientation of the silicon substrate as well as environmental conditions (e.g., humidity), which impeded the reproducibility of the Si/P3HT device. In addition, the increasing thickness of SiO_x could become a barrier for charge injection from Si to P3HT, leading to a decrease in J_{sc}. An alternative surface passivation method should be developed to overcome such charge recombination issues in P3HT/Si devices.

Methyl-Terminated (−CH_3) Planar Silicon Electrodes. Silicon surfaces have been terminated with alkyl groups to decrease the velocity of surface recombination.[35,38] The velocity of surface recombination for such surfaces can be as low as 45 cm/s, even when exposed to ambient air for more than 48 h. Here, a −CH_3−Si substrate was achieved via a two-step chlorination/methylation process. As shown in Figure 1, the EQE and PCE of the −CH_3−Si/P3HT device were improved significantly compared with the other devices. Based on the $I-V$ curve for the −CH_3−Si/P3HT device, a J_{sc} of 9.4 mA cm^{-2}, V_{oc} of 0.473 V, and FF of 0.25 gave a PCE of 1.1%. Compared with SiO_x termination, a net positive dipole was formed arising from covalent Si−C surface bonding, which generated an internal electric field. Synchrotron photoemission studies have shown that CH_3−Si surfaces possess a positive surface dipole of ~0.38 eV,[42] hence CH_3−Si(111) surfaces possess a significant electron affinity of 3.67 eV, as shown in Scheme 1b. Furthermore, from the perspective of the molecular orbital, chemical bond formation between a Si atom and methyl group produces new orbital in the Si/CH_3 system resulting from interactions between the frontier orbital of the methyl group and surface state levels of the silicon atoms. This leads to a novel highest occupied molecular orbital (HOMO)−lowest unoccupied molecular orbital (LUMO) gap in the Si/CH_3 system of 7.3 eV, which is narrower than that of the free methyl group (9−10 eV).[47]

Scheme 2. Schematic Drawing of the Structure of a Hybrid Organic−Inorganic PV Cell Containing SiNWs as Electrode[a]

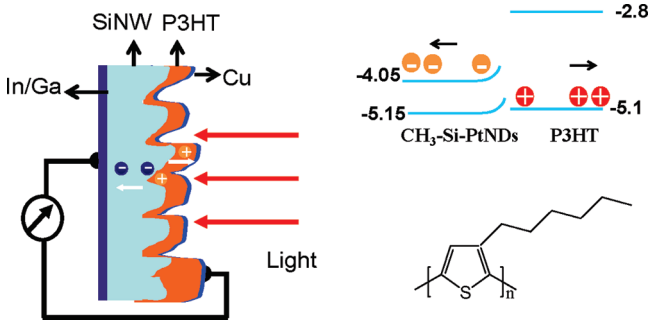

[a] The surface of the vertical SiNWs was covalently bound to methyl groups and decorated with PtNDs (not drawn here). Light passed through the top semi-transparent copper electrode and was absorbed along the length of the wire. The produced minority-carrier holes readily diffuse to the Si/P3HT junction where they undergo charge separation. The molecular structure of P3HT is shown at the bottom-right. The alignment of the electronic energy levels of the device is illustrated at the top-right.

This observation was also verified by UPS measurements, as shown in Figure 2, where the position of the valence band (VB) shifted dramatically to a more negative value (8.9 eV) compared with that of bulk silicon (5.15 eV). The offset of the electron affinity at the −CH_3−Si surface shifted ~0.35 eV compared with that of SiO_x (~0.15 eV), leading to larger driving force promoting electron movement toward the cathode. Furthermore, in case of methyl group termination, only one monolayer formed on the silicon surface, allowing more efficient charge coupling between silicon and P3HT. This layer dramatically suppresses the formation of SiO_x, even after immersing the substrate in water. Both of these advantages resulted in the superior performance of the hybrid −CH_3−Si/P3HT devices.

Methyl-Terminated Silicon Nanowire Array (−CH_3−SiNW) Electrodes. Although a PCE of 1.1% was achieved by lowering the velocity of surface recombination, compared with alternative hybrid devices (e.g., CdSe/P3HT), this value was still modest even though silicon possesses wide absorption window to harvest light. In an attempt to further increase the PCE, a device configuration was proposed (as shown in Scheme 2) that has the following advantages: (i) The SiNWs architecture provides a direct pathway for electron carriers. Meanwhile, holes diffuse in the radial direction of the SiNWs to P3HT. (ii) The vertical SiNWs architecture decouples charge carrier collection from light absorption. Light is absorbed along the long axis of the SiNWs, whereas holes diffuse the radial distance to the Si/P3HT interface. (iii) Two complementary photon absorbers generate the total photocurrent, namely, SiNWs and P3HT. A hybrid device with this architecture of vertically oriented SiNWs providing a large interfacial area and high light harvesting capability was fabricated.

The use of long SiNWs combined with P3HT for PV devices was initially explored. Cross-sectional and top view SEM images of the SiNWs are shown in Figure S2 in the Supporting Information. The SiNWs exhibited a uniform alignment with an axial-orientation with a length of ~10 μm. However, this PV device displayed very poor performance (not shown here). The SiNWs were too long to allow P3HT to penetrate into the bottom spaces between the SiNWs. Meanwhile, the holes

dx.doi.org/10.1021/cm103221a |*Chem. Mater.* 2011, 23, 2084–2090

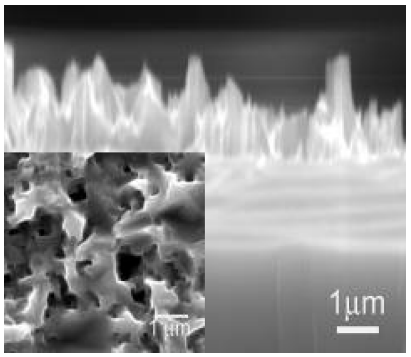

Figure 3. Cross-sectional SEM image of shortened SiNWs. Inset: top view of the surface of the SiNWs.

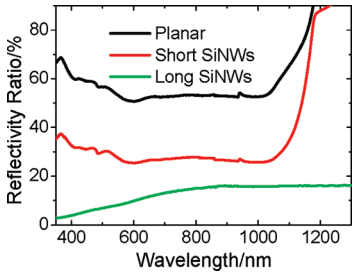

Figure 4. Light reflectivity ratios of a planar silicon substrate, long SiNWs and short SiNWs.

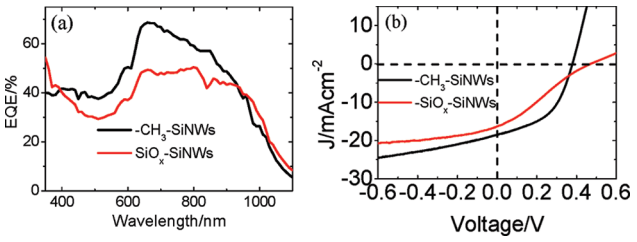

Figure 5. (a) EQE and (b) $I-V$ curves of hybrid devices containing SiNWs with various surface modifications.

presented in P3HT but far from the anode could not be collected because of its modest charge transport capability. To allow P3HT to access the spaces between SiNWs, the SiNWs were shortened. As shown in Figure 3b, the length of the SiNWs was decreased from ca. ten micrometers to a few hundred nanometers. This allowed P3HT to readily access the spaces between the shorter SiNWs. Compared with the long SiNWs, the short ones still displayed a relatively low light reflection ratio of 30%, as shown in Figure 4.

As shown in Figure 5, a hybrid cell based on $-CH_3-$SiNWs displayed dramatic improvement over the $-CH_3-$Si device, as did that based on $-SiO_x-$SiNWs. Like the planar silicon electrode, passivation with a methyl surface gave superior PV performance compared with passivation of oxide. The EQE of the $-CH_3-$SiNWs device reached 69%, while 49% was achieved for the $-SiO_x-$SiNWs device. The $-CH_3-$SiNWs device showed a J_{sc} of 18.5 mA cm^{-2}, V_{oc} of 0.379 V, FF of 0.48, and PCE of 3.4%, while the PCE of the $-SiO_x-$SiNWs cell was 2.0%. Obviously, J_{sc} was higher in the SiNWs devices compared with that of devices containing a planar silicon electrode, which was

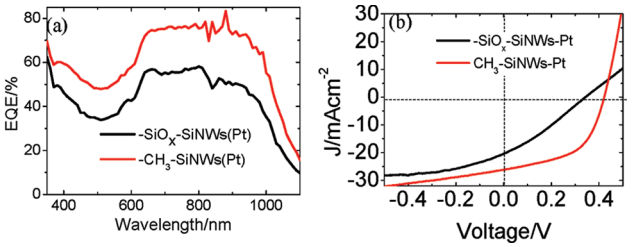

Figure 6. (a) EQE and (b) $I-V$ curves of hybrid devices containing SiNWs with various surface modifications and PtNDs.

Table 1. Response of Hybrid PV Cells Containing Different Silicon Electrodes under Simulated AM 1.5 Solar Irradiation at 100 mW/cm^2

devices	J_{sc} (mA/cm^2)	V_{oc} (V)	FF	PCE (%)
$-$H$-$ planar silicon	0.031	0.458	0.41	0.006
$-SiO_x-$ planar silicon	6.8	0.448	0.30	0.9
$-CH_3-$ planar silicon	9.4	0.473	0.25	1.1
$-SiO_x-$SiNWs	16.3	0.470	0.26	2.0
$-CH_3-$SiNWs	18.5	0.379	0.48	3.4
$-SiO_x-$SiNWs(Pt)	20.5	0.343	0.30	2.1
-CH_3-SiNWs(Pt)	26.2	0.421	0.53	5.9

assigned to more efficient light harvesting and a larger interface for charge generation. In the SiNWs/P3HT device, the EQE spectrum showed that the photocurrent was mainly derived from silicon instead of P3HT. Although there was a large organic/inorganic interface where excitons in P3HT underwent charge transfer, the short exciton diffusion length in P3HT limited the final photocurrent.[2,43−46] Much of the light harvested by P3HT generated excitons that could not reach the organic/inorganic interface to undergo charge separation because of the short exciton diffusion length.

Decoration with PtNDs. Surface modification with organic groups does not proceed completely, so pinhole areas covered with Si−H might still remain on a methylated silicon surface.[41,48] In a previous report, Pt nuclei only formed via electrochemical deposition at the holes in the attached organic layer on alkyl-modified *n*-Si.[48] Electrodeposition of Pt on Si from a solution of $[PtCl_6]^{2-}$ in ethanol was expected to occur via adsorption of $[PtCl_4]^{2-}$ ions. PtNDs played two critical roles at this organic−inorganic interface. First, hydrogen bonds were replaced with PtNDs in the pinhole areas, which decreases the velocity of surface recombination. Devices based on electrodes formed from gold nanodots deposited on SiNWs in our further investigation displayed a similar enhancement compared with that lacking metal nanodots, which verifies the above mechanism. Vacuum deposition has the reverse effect on device performance because of nonselective metal deposition. During vacuum deposition, Pt can be deposited anywhere on the Si surface, which leads to a high density of crystalline nuclei for Pt growth. Second, UPS measurements revealed that deposition of PtNDs led to the formation of an even larger favorable internal electric field, as shown in Scheme 1b and Figure 2. The offset of surface electron affinity ($-CH_3-$Si(Pt)) was ~0.65 eV compared with 0.35 eV for the device without Pt. Hence, the driving force for electron movement toward the anode increased with Pt deposition. According to Figure 6 and Table 1, the PV cell containing

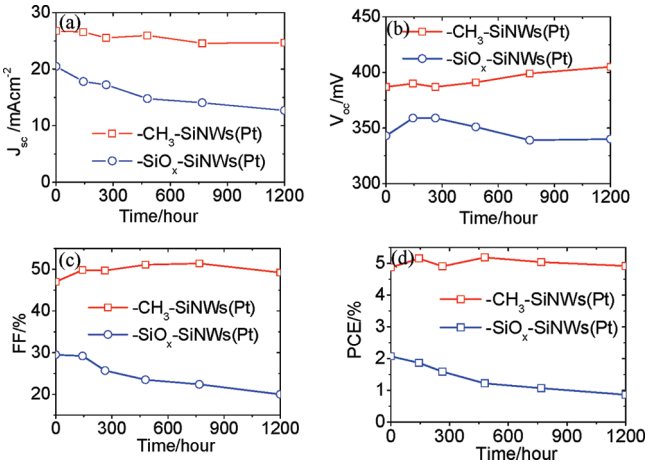

Figure 7. Stability of hybrid devices based on SiO_x− and CH_3− terminated SiNWs with deposited PtNDs. Changes in (a) J_{sc}, (b) V_{oc}, (c) FF, and (d) PCE over time.

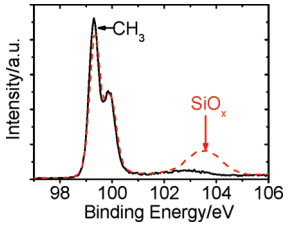

Figure 8. XPS measurements of Si(2p) peaks for SiO_x− (dashed line) and CH_3− terminated (solid line) Si(100) surfaces. The solid line showed Si(2p) emission for the CH_3-terminated Si surface, where the peaks at 99 and 100 eV were from silicon. The dashed line showed Si(2p) emission for the SiO_x-terminated Si surface, where the peaks at 99 and 100 eV were ascribed to silicon and the peak at 103 eV was ascribed to oxidized silicon.

−CH_3−SiNWs decorated with PtNDs (−CH_3−SiNWs(Pt)) exhibited a J_{sc} of 26.2 mA cm^{-2}, V_{oc} of 0.421 V, and FF of 0.53, giving a PCE of 5.9%. In contrast, the device based on −SiO_x−SiNWs(Pt)/P3HT displayed a PCE of 2.1%, which is similar to that of the device without PtNDs (2.0%) because of the uncontrolled deposition of PtNDs.

Stability of PV Devices. The stability of hybrid devices is critical for their future application. The performance of devices based on −SiO_x−SiNWs(Pt)/P3HT and −CH_3−SiNWs(Pt)/P3HT over time is shown in Figure 7. After 1200 h aging, the J_{sc} of the device fabricated from a −CH_3−SiNWs(Pt) electrode displayed negligible decay, as did the FF, while V_{oc} increased. The PCE did not show any degradation. In contrast, J_{sc} and FF of the device based on a −SiO_x−SiNWs(Pt) electrode decreased significantly, while V_{oc} remained unchanged. The PCE of the −SiO_x−SiNWs(Pt) device decreased from an initial 2.1% to 0.8% after 1200 h. The degradation of this device was ascribed to the presence of an uncontrolled SiO_x layer. The thickness of this layer gradually increased over time to form a larger charge injection/transfer barrier. However, XPS analysis revealed that no SiO_x was present on the CH_3-terminated silicon surface (Figure 8). After methylation, only a negligible signal from SiO_x was observed. In contrast, a large signal from SiO_x was detected for the silicon substrate that was not methylated.

CONCLUSIONS

In conclusion, the organic−inorganic P3HT−silicon interface in hybrid devices played a critical role in their performance. Both formation of a thin SiO_x layer and termination with methyl groups enhanced the PCE of hybrid devices because the velocity of surface recombination was suppressed and a favorable internal electric field formed. A hybrid device based on a −CH_3 silicon electrode displayed a higher PCE than that containing a SiO_x one because of a larger internal electric field. SiNWs dramatically improved the PCE of hybrid devices, which was ascribed to their strong light harvesting capability and optimized charge transport pathways. In addition, decoration of the SiNWs with PtNDs further enhanced the PCE of hybrid devices, which was attributed to a larger net positive dipole as well as passivation specifically at nonalkylated sites. A maximum PCE of 5.9% was achieved for the −CH_3−SiNWs(Pt) device under simulated AM 1.5 solar radiation at 100 mW cm^{-2} as well as stable performance after illumination for >1000 h. In contrast, a device based on a −SiO_x−SiNWs(Pt) electrode exhibited poor stability because the thickness of the SiO_x layer increased over time. This investigation indicated that stable organic−inorganic hybrid PV devices with a high PCE can be achieved by facile surface modification.

ASSOCIATED CONTENT

Supporting Information. The formation of a SiO_x layer on a freshly prepared hydrogen-terminated silicon substrate, time dependence of J_{sc} of an uncapsulated device based on −H−Si/P3HT immediately after removal from a glovebox under simulated AM 1.5 solar irradiation at 100 mW cm^{-2}, and top and cross-sectional view SEM images of long SiNWs. This material is available free of charge via the Internet at http://pubs.acs.org.

AUTHOR INFORMATION

Corresponding Author

*E-mail: bqsun@suda.edu.cn. Fax: 0086-512-65882846. Tel: 0086-512-65880951.

ACKNOWLEDGMENT

This work was supported by the National Basic Research Program of China (973 Program) (Grant No. 2010CB934502), National Natural Science Foundation of China (Grant No. 60976050), the Fok Ying Tung Education Foundation (Grant 114022), Research Grants Council of Hong Kong SAR-CRF Grant (Grant CityU5/CRF/08), and Joint research project of RGC and NSFC (Grant N_CityU108/08).

REFERENCES

(1) Greenham, N. C.; Peng, X. G.; Alivisatos, A. P. *Phys. Rev. B* **1996**, *54*, 17628.
(2) Gunes, S.; Neugebauer, H.; Sariciftci, N. S. *Chem. Rev.* **2007**, *107*, 1324.
(3) Huynh, W. U.; Dittmer, J. J.; Alivisatos, A. P. *Science* **2002**, *295*, 2425.
(4) Saunders, B. R.; Turner, M. L. *Adv. Colloid Interface Sci.* **2008**, *138*, 1.
(5) Dayal, S.; Kopidakis, N.; Olson, D. C.; Ginley, D. S.; Rumbles, G. *Nano Lett.* **2010**, *10*, 239.

(6) Sun, B. Q.; Marx, E.; Greenham, N. C. *Nano Lett.* **2003**, *3*, 961.
(7) Boucle, J.; Chyla, S.; Shaffer, M. S. P.; Durrant, J. R.; Bradley, D. D. C.; Nelson, J. *Adv. Funct. Mater.* **2008**, *18*, 622.
(8) Ravirajan, P.; Haque, S. A.; Durrant, J. R.; Bradley, D. D. C.; Nelson, J. *Adv. Funct. Mater.* **2005**, *15*, 609.
(9) Beek, W. J. E.; Wienk, M. M.; Janssen, R. A. J. *Adv. Mater.* **2004**, *16*, 1009.
(10) McDonald, S. A.; Konstantatos, G.; Zhang, S. G.; Cyr, P. W.; Klem, E. J. D.; Levina, L.; Sargent, E. H. *Nat. Mater.* **2005**, *4*, 138.
(11) Cui, D. H.; Xu, J.; Zhu, T.; Paradee, G.; Ashok, S.; Gerhold, M. *Appl. Phys. Lett.* **2006**, *88*, 183111.
(12) Sun, B. Q.; Zou, G. F.; Shen, X. J.; Zhang, X. H. *Appl. Phys. Lett.* **2009**, *94*, 233504.
(13) Adikaari, A. A. D. T.; Dissanayake, D. M. N. M.; Hatton, R. A.; Silva, S. R. P. *Appl. Phys. Lett.* **2007**, *90*, 203514.
(14) Alet, P. J.; Palacin, S.; Cabarrocas, P. R. I.; Kalache, B.; Firon, M.; Bettignies, R. D. *Eur. Phys. J.: Appl. Phys.* **2006**, *36*, 231.
(15) Liu, C. Y.; Holman, Z. C.; Kortshagen, U. R. *Nano Lett.* **2009**, *9*, 449.
(16) Nolasco, J. C.; Cabre, R.; Ferre-Borrull, J.; Marsal, L. F.; Estrada, M.; Pallares, J. *J. Appl. Phys.* **2010**, *107*, 044505.
(17) Shiu, S. C.; Chao, J. J.; Hung, S. C.; Yeh, C. L.; Lin, C. F. *Chem. Mater.* **2010**, *22*, 3108.
(18) Shen, X.; Sun, B.; Yan, F.; Zhao, J.; Zhang, F.; Wang, S.; Zhu, X.; Lee, S. *ACS Nano* **2010**, *4*, 5869.
(19) Kelzenberg, M. D.; Boettcher, S. W.; Petykiewicz, J. A.; Turner-Evans, D. B.; Putnam, M. C.; Warren, E. L.; Spurgeon, J. M.; Briggs, R. M.; Lewis, N. S.; Atwater, H. A. *Nat. Mater.* **2010**, *9*, 239.
(20) Boettcher, S. W.; Spurgeon, J. M.; Putnam, M. C.; Warren, E. L.; Turner-Evans, D. B.; Kelzenberg, M. D.; Maiolo, J. R.; Atwater, H. A.; Lewis, N. S. *Science* **2010**, *327*, 185.
(21) Garnett, E. C.; Yang, P. D. *J. Am. Chem. Soc.* **2008**, *130*, 9224.
(22) Goodey, A. P.; Eichfeld, S. M.; Lew, K. K.; Redwing, J. M.; Mallouk, T. E. *J. Am. Chem. Soc.* **2007**, *129*, 12344.
(23) Peng, K. Q.; Xu, Y.; Wu, Y.; Yan, Y. J.; Lee, S. T.; Zhu, J. *Small* **2005**, *1*, 1062.
(24) Sivakov, V.; Andra, G.; Gawlik, A.; Berger, A.; Plentz, J.; Falk, F.; Christiansen, S. H. *Nano Lett.* **2009**, *9*, 1549.
(25) Tian, B. Z.; Zheng, X. L.; Kempa, T. J.; Fang, Y.; Yu, N. F.; Yu, G. H.; Huang, J. L.; Lieber, C. M. *Nature* **2007**, *449*, 885.
(26) Zhu, J.; Yu, Z. F.; Burkhard, G. F.; Hsu, C. M.; Connor, S. T.; Xu, Y. Q.; Wang, Q.; McGehee, M.; Fan, S. H.; Cui, Y. *Nano Lett.* **2009**, *9*, 279.
(27) Hu, L.; Chen, G. *Nano Lett.* **2007**, *7*, 3249.
(28) Huang, J. S.; Hsiao, C. Y.; Syu, S. J.; Chao, J. J.; Lin, C. F. *Sol. Energy Mater. Sol. Cells* **2009**, *93*, 621.
(29) Muskens, O. L.; Rivas, J. G.; Algra, R. E.; Bakkers, E.; Lagendijk, A. *Nano Lett.* **2008**, *8*, 2638.
(30) Kalita, G.; Adhikari, S.; Aryal, H. R.; Afre, R.; Soga, T.; Sharon, M.; Koichi, W.; Umeno, M. *J. Phys. D: Appl. Phys.* **2009**, *42*, 5.
(31) Williams, E. L.; Jabbour, G. E.; Wang, Q.; Shaheen, S. E.; Ginley, D. S.; Schiff, E. A. *Appl. Phys. Lett.* **2005**, *87*, 223504.
(32) Garnett, E. C.; Yang, P. *Nano Lett.* **2010**, *10*, 1082.
(33) Boettcher, S. W.; Spurgeon, J. M.; Putnam, M. C.; Warren, E. L.; Turner-Evans, D. B.; Kelzenberg, M. D.; Maiolo, J. R.; Atwater, H. A.; Lewis, N. S. *Science* **2010**, *327*, 185.
(34) Kayes, B. M.; Atwatera, H. A.; Lewis, N. S. *J. Appl. Phys.* **2005**, *97*, 114302.
(35) Sieval, A. B.; Huisman, C. L.; Schonecker, A.; Schuurmans, F. M.; van der Heide, A. S. H.; Goossens, A.; Sinke, W. C.; Zuilhof, H.; Sudholter, E. J. R. *J. Phys. Chem. B* **2003**, *107*, 6846.
(36) Godfrey, R. B.; Green, M. A. *Appl. Phys. Lett.* **1979**, *34*, 790.
(37) Fossum, J. G.; Burgess, E. L. *Appl. Phys. Lett.* **1978**, *33*, 238.
(38) Maldonado, S.; Knapp, D.; Lewis, N. S. *J. Am. Chem. Soc.* **2008**, *130*, 3300.
(39) Peng, K. Q.; Yan, Y. J.; Gao, S. P.; Zhu, J. *Adv. Mater.* **2002**, *14*, 1164.
(40) Bansal, A.; Li, X. L.; Lauermann, I.; Lewis, N. S.; Yi, S. I.; Weinberg, W. H. *J. Am. Chem. Soc.* **1996**, *118*, 7225.
(41) Maldonado, S.; Plass, K.; Knapp, D.; Lewis, N. *J. Phys. Chem. C* **2007**, *2007*, 17690.
(42) Hunger, R.; Fritsche, R.; Jaeckel, B.; Jaegermann, W.; Webb, L.; Lewis, N. *Phys. Rev. B* **2005**, *72*, 45317.
(43) Halls, J. J. M.; Pichler, K.; Friend, R. H.; Moratti, S. C.; Holmes, A. B. *Synth. Met.* **1996**, *77*, 277.
(44) Haugeneder, A.; Neges, M.; Kallinger, C.; Spirkl, W.; Lemmer, U.; Feldmann, J.; Scherf, U.; Harth, E.; Gugel, A.; Mullen, K. *Phys. Rev. B* **1999**, *59*, 15346.
(45) Pettersson, L. A. A.; Roman, L. S.; Inganas, O. *J. Appl. Phys.* **1999**, *86*, 487.
(46) Stubinger, T.; Brutting, W. *J. Appl. Phys.* **2001**, *90*, 3632.
(47) Salomon, A.; Boecking, T.; Seitz, O.; Markus, T.; Amy, F.; Chan, C.; Zhao, W.; Cahen, D.; Kahn, A. *Adv. Mater.* **2007**, *19*, 445.
(48) Takabayashi, S.; Ohashi, M.; Mashima, K.; Liu, Y.; Yamazaki, S.; Nakato, Y. *Langmuir* **2005**, *21*, 8832.